Parametric modelling and dynamic characterization of a two-degree-of-freedom twin-rotor multi-input multi-output system

S M Ahmad, A J Chipperfield and **M O Tokhi***
Department of Automatic Control and Systems Engineering, University of Sheffield, UK

Abstract: A mathematical model for the dynamic characterization of a two-degree-of-freedom (2 DOF) twin-rotor multi-input multi-output (MIMO) system (TRMS) in hover is extracted using a black box system identification technique. The behaviour of the TRMS, in certain aspects, resembles that of a helicopter, with a significant cross-coupling between longitudinal and lateral directional motions. Hence, it is an interesting identification and control problem. Identification for a 2 DOF, rigid-body, discrete-time linear model is presented in detail. The extracted model has a good degree of prediction capability. The modelling approach presented is suitable for complex new-generation air vehicles.

Keywords: discrete-time systems, helicopter, MIMO linear identification, time and frequency domain analysis, TRMS

NOTATION

a_i, b_i, c_i	unknown parameters to be identified
ARMAX	autoregressive moving average with exogenous input model
d.c.	direct current
$e(t)$	zero mean white noise
f	frequency (Hz)
F_1, F_2	thrust generated by the rotors in the vertical and horizontal planes respectively
G_{yx}	transfer function between output y and input x
n_a, n_b, n_c	orders of polynomials A, B and C of the ARMAX model
S_{xx}, S_{yy}	auto power spectral densities of input and output signals respectively
S_{xy}	cross-spectral density between a pair of input and output signals
TRMS	twin-rotor multi-input multi-output system
$u_1(t)$	input to the main rotor (V)
$u_2(t)$	input to the tail rotor (V)
$y_1(t)$	pitch angle (rad)
$y_2(t)$	yaw angle (rad)
$\gamma^2_{xy}(f)$	ordinary coherence function
$\varepsilon(t)$	prediction errors or residuals

The MS was received on 19 July 2000 and was accepted after revision for publication on 10 January 2001.
**Corresponding author: Department of Automatic Control and Systems Engineering, University of Sheffield, Mappin Street, Sheffield S1 3JD, UK.*

1 INTRODUCTION

Research on unconventional aircraft, such as tilt rotor, tilt wing, delta-wing, canard control surfaces, X-wing, tilt body, different types of light and micro and hand-held unmanned aerial vehicles (UAVs), has assumed increased importance in recent years. This can be attributed to the increasing emphasis on the aircraft being, for example, stealth, agile, multipurpose and autonomous, for varied civilian and military operations. However, modelling details of these vehicles are highly involved and generally not reported owing to the classified nature of such projects. Moreover, the flight mechanics equations are not always easy to establish from first principles for a non-standard aircraft configuration. However, these equations are imperative for designing and studying flight control systems. In most classical fixed and rotary wing aircraft, the role of system identification is to estimate the parameters of linearized six-degree-of-freedom (6 DOF) equations of motion from flight or wind-tunnel data. Here, the structure is known and the parameters of the model have some physical meaning and are often called stability and control derivatives. These derivatives are functions of the altitude and Mach number of the aircraft and therefore would change at different operating conditions. This is true for most classical fixed and rotary wing aircraft. There is a vast number of papers addressing parameter estimation techniques for conventional aircraft [**1**, **2**]. System identification is a viable alternative for modelling unconventional aircraft, where both model structure and model parameters are unknown and need to

be identified. Modelling of such vehicles is the subject of this paper.

A number of UAVs, such as Bluebird [3], Frog [4], Solus [5] and Raven-2 [6], have been reported recently. These are based on conventional aircraft aerodynamics design philosophy. The dynamic models of these aircraft have been derived from first principles through determination of the aerodynamic stability and control derivatives, with usual decoupling of longitudinal and lateral dynamics. A literature survey has revealed many other unconventional but fascinating experimental air vehicles, some of which are briefly discussed below. These innovative platforms or 'next-generation air vehicles' are designed for specific applications and differ significantly from their classical counterparts. Recently, a considerable amount of research effort has been devoted to different modelling and control aspects of these exotic vehicles. A free wing [7] UAV is modelled using conventional mathematical modelling techniques. The Caltech ducted fan laboratory aircraft [8] has accordingly been developed to demonstrate control techniques for hover to forward flight transition for the thrust-vectored aircraft. Modelling and control of a radio-controlled (RC) laboratory helicopter has been reported in reference [9], where modern identification and robust control techniques have been investigated for the hover mode. Identification of the autogyro (gyroplane), a popular sport and recreational flying machine, has been documented in reference [10]. Werner *et al.* [11] have developed a mathematical model from first principles for a 2 DOF laboratory aircraft. This plant was developed primarily to model the behaviour of a vertical-take-off plane. Non-linear system identification techniques such as neural networks have been applied in the modelling of an Ariel UAV [12]. Neural networks were also employed for the wind-tunnel wing model at NASA [13]. It is evident from the above cases that the plant is modelled using classical mathematical modelling based on the analysis of plant aerodynamics, i.e. using laws of physics. Furthermore, the parameters of the model are either known or obtained using linear or non-linear system identification techniques. However, the modelling technique presented in this paper is suitable for a wide range of new-generation air vehicles whose flight dynamics are either difficult to obtain via mathematical modelling or not easily understood. The modelling is done assuming no prior knowledge of the model structure or parameters relating to physical phenomena, i.e. black box modelling.

This paper addresses modelling of an experimental test rig, representing a complex 2 DOF twin-rotor multi-input multi-output (MIMO) system (TRMS) using system identification techniques. The authors' previous work [14, 15] has addressed the modelling of a 1 and 2 DOF TRMS.

The paper is organized as follows: Section 2 explains the motivation that prompted this study, Section 3 describes the experimental set-up, Section 4 delineates the experimentation and data analysis, Section 5 presents the results, a physical interpretation of the black box models is given in Section 6 and the paper is concluded in Section 7.

2 MOTIVATION

The motivation for this work stems from the fact that the behaviour of the TRMS (Fig. 1) in certain aspects resembles that of a helicopter. The TRMS is a laboratory set-up designed for control experiments by Feedback Instruments Limited [16]. From the control point of view it exemplifies a high-order non-linear system with significant cross-coupling. The main differences between the helicopter and the TRMS are:

1. In a single main rotor helicopter the pivot point is located at the main rotor head, whereas in case of the TRMS pivot point it is mid-way between the two rotors.
2. In a helicopter, lift is generated via collective pitch

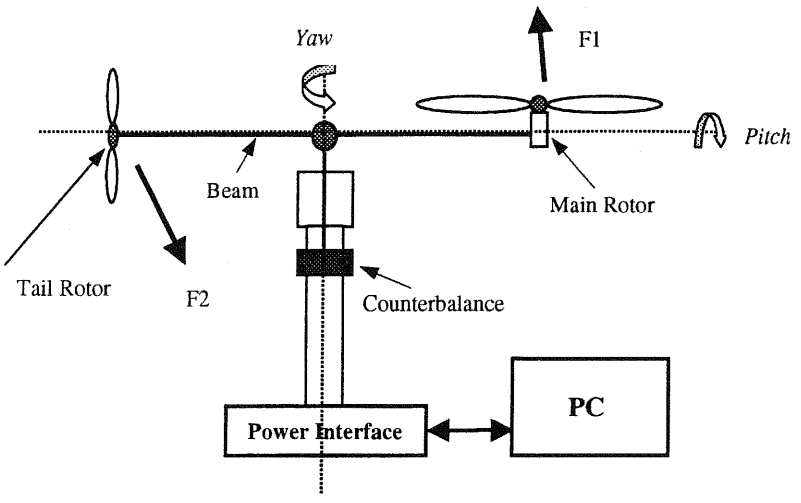

Fig. 1 Twin-rotor MIMO system

control; i.e. pitch angles of all the blades of the main rotor are changed by an identical amount at every point in azimuth, but at constant rotor speed. However, in the case of the TRMS, pitch angles of all the blades are fixed and speed control of the main rotor is employed to achieve vertical control.

3. Similarly, yaw is controlled in a helicopter by changing, by the same amount, the pitch angle of all the blades of the tail rotor. In the TRMS, yawing is affected by varying the tail rotor speed.
4. There are no cyclical controls in the TRMS: cyclic control is used for directional control in a helicopter.

However, as in a helicopter, there is strong cross-coupling between the collective (main rotor) and the tail rotor in the TRMS.

Hovering is vital for a variety of flight missions, such as load delivery, air/sea rescue and surveillance. Yet maintaining a station is one of the difficult problems in helicopter flight, because in this mode, the dynamically unstable helicopter is flying at near-zero forward speed. Although the TRMS rig reference point is fixed, it still resembles a helicopter by being highly non-linear with strongly coupled modes. The hovering property of a helicopter/TRMS is the main area of interest in this work. Station keeping of a plant is thus a good benchmark problem to test and explore modern identification and control methodologies. The experimental set-up simulates similar problems and challenges encountered in real systems. These include complex dynamics leading to both parametric and dynamic uncertainty, unmeasurable states, sensor and actuator noise, saturation and quantization, bandwidth limitations and delays.

In this paper, attention is focused on the identification and verification of longitudinal and lateral dynamics of a 2 DOF TRMS with its main beam (body) in a flat horizontal position representing hover mode. The primary interest lies in the identification of low-frequency (0–1 Hz) dynamic modes corresponding to rigid-body and rotor dynamics of the TRMS, as is the case with helicopters [**17**]. A quantitative and qualitative approach is presented that utilizes time and frequency response comparison of the simulation model. The goal of the validation effort is to increase confidence in the fidelity of the model for use in various research applications such as simulation of rigid-body motion, model validation, vibration suppression and control design. The future work will investigate some of these aspects.

3 EXPERIMENTAL SET-UP

The TRMS (Fig. 1) consists of a beam pivoted on its base in such a way that it can rotate freely both in its horizontal and vertical planes. There are rotors (the main and tail rotors), driven by d.c. motors, at both ends of the beam. A counterbalance arm with a weight at its end is fixed to the beam at the pivot. The state of the beam is described by four process variables: horizontal and vertical angles measured by position sensors fitted at the pivot, and two corresponding angular velocities. Two additional state variables are the angular velocities of the rotors, measured by tachogenerators coupled to the driving d.c. motors. The system permits both 1 and 2 DOF experiments.

In a typical helicopter, the aerodynamic force is controlled by changing the angle of attack of the blades. The laboratory set-up is constructed so that the angle of attack of the blades is fixed. The aerodynamic force is controlled by varying the speed of the motors. Therefore, the control inputs are supply voltages of the d.c. motors. A change in the voltage value results in a change in the rotational speed of the propeller, which results in a change in the corresponding position of the beam [**16**]. F_1 and F_2 in Fig. 1 represent the thrust generated by the rotors in the vertical and horizontal planes respectively.

4 EXPERIMENTATION

The objective of the identification experiments is to estimate a linear time-invariant (LTI) model of the 2 DOF TRMS in hover without any prior system knowledge pertaining to the exact mathematical model structure. No model structure is assumed *a priori*, unlike aircraft system identification where the identification procedure is reduced to estimating the coefficients of a set of differential equations describing the aircraft dynamics. The differential equations describe the external forces and moments in terms of accelerations and state and control variables, where the coefficients are the stability and control derivatives. The extracted model is to be utilized for low-frequency vibration control and design of a suitable feedback control law for disturbance rejection and reference tracking. Hence, accurate identification of low-frequency rigid-body dynamic modes is imperative. This would also facilitate understanding of the dominant modes of the TRMS. Since no mathematical model is available, a level of confidence has to be established in the identified model through rigorous frequency and time domain analyses and cross-validation tests.

It is intuitively assumed that the body resonance modes of the TRMS lie in a low-frequency range of 0–1 Hz, while the main rotor dynamics is at significantly higher frequencies. The rig configuration is such that it permits open-loop system identification, unlike a helicopter which is open-loop unstable in hover mode. In Fig. 2, the input signals u_1 and u_2 represent voltage inputs to the main rotor and tail rotor respectively. The outputs y_1 and y_2 represent pitch and yaw angles respectively. Strong coupling exists between the two channels, and this may be accounted for by representing the dynamics of the TRMS by the multivariable transfer function model as given in Fig. 2.

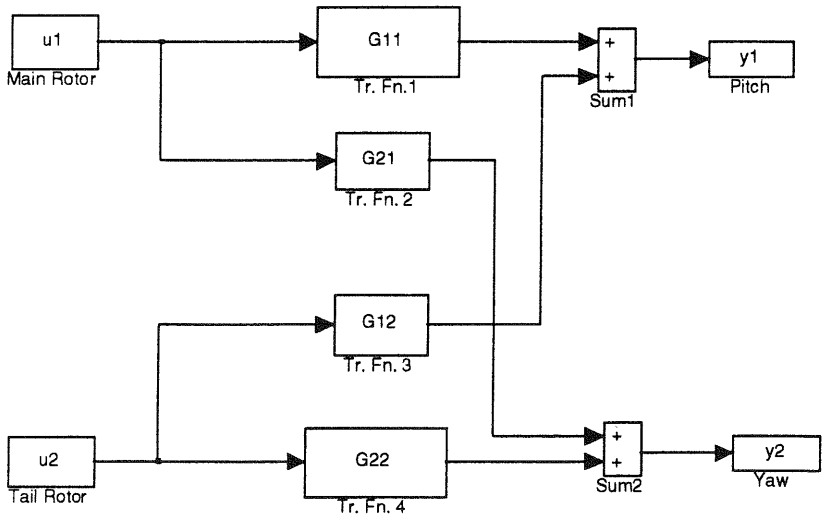

Fig. 2 MIMO transfer function model

4.1 Flight test database

The TRMS has been upgraded, and joy stick control analogous to that of a helicopter pilot stick is provided. Test signals could be applied using the stick, but only a very simple signal sequence is feasible and this is insufficient to ensure adequacy of spectral content and repeatability. Moreover, the system is very sensitive and precise control cannot be exercised. Hence, the test signal is designed separately and read from the workspace in the MATLAB/SIMULINK environment, instead of using the stick. This is analogous to automation of the test signal, which ensures that the experiments are sufficiently controlled and repeatable, and guarantees the desired spectral content.

The trim configuration was the steady state horizontal position of the beam of the TRMS. Since the TRMS is very sensitive to atmospheric disturbances, the tests were conducted in practically calm air. Having established trim, a predesigned input signal is given to one control at a time. In order to excite the rigid-body modes of interest, i.e. up to 1 Hz, a pseudo-random binary sequence (PRBS) signal of 2 Hz band limit and of small amplitude is applied to the controls so that the system remains in its linear operating region around the selected equilibrium (trim) point. The PRBS signal used in this work is shown in Fig. 8a. A simple approach is adopted, where the first channel is excited using the PRBS while the input to the second channel is held constant and responses are measured for the two outputs. The steady state effects of the second constant input signal on the first and second outputs, via the transfer functions G_{12} and G_{22}, are removed prior to fitting the model between the $u_1 \rightarrow y_1$ and $u_1 \rightarrow y_2$ channels. The experiments were then repeated for the second channel by keeping the first input constant. Similarly, the steady state influence of the first input on the first and second outputs, through the transfer functions G_{11} and G_{21}, are removed prior to fitting the model between the $u_2 \rightarrow y_1$ and $u_2 \rightarrow y_2$ channels. This is accomplished by subtracting the mean values from the corresponding output signals.

4.2 Data reliability and sampling analyses

Measurements used for system identification were pitch position y_1, azimuth or yaw position y_2 (in radians) and controls u_1 and u_2 (in volts). The measured data were sampled and recorded on a PC using real-time kernel (RTK) software. Data quality and consistency are critical to the identification. Excessively noisy or kinematically inconsistent data may lead to identification of an incorrect model. Preliminary checks of data quality and consistency can ensure that these sources of error are minimized. The TRMS is very sensitive to atmospheric disturbances and, in order to ensure accurate identification, each signal was repeated many times until a response, undisturbed by gusts of air, was obtained.

The duration of the test signal was 120 s and a sampling interval of 10 Hz was chosen as the sampling frequency; 10 times the guessed bandwidth is found to be a good choice in most cases [**18**]. An excessively fast sampling rate leads to a non-minimum phase system and poles clustered around the unit circle. Poles close to the origin indicate that the sampling rate is too slow [**19**]. Although it has been shown in an earlier work by the present authors [**20**] that 5 Hz sampling is good enough to capture the main system dynamics, a sampling period of 10 Hz is employed in this case. The reason for this is that frequency domain data analysis, as carried out in this work, in particular coherence function calculation, requires a large number of data points in order to avoid resolution bias error [**21**].

4.3 Coherence test for linearity

It is important in linear system identification to keep the effects of non-linearities to a minimum. The coherence is a

measure of the linear dependence of the output on the input, defined in spectral terms; i.e. it expresses the degree of linear correlation in the frequency domain between the input and the output signal. An important use of the coherence spectrum is its application as a test of signal–noise ratio and linearity between one or more input variables and an output variable. The coherence function, $\gamma^2_{xy}(f)$, is given by

$$\gamma^2_{xy}(f) = \frac{|S_{xy}(f)|^2}{S_{xx}(f)S_{yy}(f)} \tag{1}$$

where S_{xx} and S_{yy} are the autospectral densities of the input and output signals respectively and S_{xy} is the cross-spectral density between the input and the output signals. By definition, the coherence function lies between 0 and 1 for all frequencies f:

$$0 \leqslant \gamma^2_{xy}(f) \leqslant 1$$

If $x(t)$ and $y(t)$ are completely unrelated, the coherence function will be zero, while a totally noise-free linear system would yield $\gamma^2_{xy}(f) = 1$. The coherence function may thus be viewed as a type of correlation function in the frequency domain where a coherence function not equal to 1 indicates the presence of one or more of the following [**21**]:

1. Extraneous noise is present in the input and the output measurements.
2. The system relating $x(t)$ and $y(t)$ is not linear.
3. The output $y(t)$ is due to an input $x(t)$ as well as other inputs such as external disturbances.
4. Resolution bias errors are present in the spectral estimates.

When a system is noisy or non-linear, the coherence function indicates the accuracy of a linear identification as a function of frequency. The closer it is to unity at a given frequency, the more reliance can be placed on an accompanying frequency response estimate at that frequency. For a real application, which will be non-linear and affected, to some extent, by noise, a plot of the coherence function against frequency will indicate the way in which the disturbances change across the frequency band. A coherence test is employed on all the input–output data channels and is discussed next.

The linearity of the operating region is confirmed by a flat coherence of unity between the input PRBS signal and the output responses. Coherence spectra for the four channels are shown in Fig. 3. Good excitation was achieved from 0–1 Hz, which includes all the important rigid-body and main rotor dynamic modes. Strong interaction was observed among the channels $u_1 \rightarrow y_1$, $u_1 \rightarrow y_2$ and $u_2 \rightarrow y_2$, but not the $u_2 \rightarrow y_1$ channel. Non-interaction between $u_2 \rightarrow y_1$ is clearly visible from Fig. 4, as there is negligible pitch movement y_1 due to the PRBS input u_2. Strong coupling is manifest from a coherence spectrum of near unity for the $u_1 \rightarrow y_1$, $u_1 \rightarrow y_2$ and $u_2 \rightarrow y_2$ routes at most frequencies of interest, i.e. 0–1 Hz. Since no strong coherence exists in the $u_2 \rightarrow y_1$ channel, this channel was not investigated further for model fitting.

5 RESULTS

This section discusses the identification of the TRMS, which involves three steps: characterization, identification and verification.

5.1 Mode or structure determination

Theoretically, the TRMS will have an infinite number of normal modes with associated frequencies. However, it is intuitively assumed that the main dynamics (modes) of the TRMS lie in the 0–1 Hz range. It is further assumed that the rotor dynamics are at significantly higher frequencies than the rigid-body modes. Hence, these can be neglected and the rotor influence is lumped into the rigid-body derivatives. Under these broad hypotheses, investigations are carried out to characterize the behaviour of the TRMS through a series of experiments.

The coherence spectra in Fig. 3 and spectral density analyses of the system revealed that the information is good for most frequencies up to 1 Hz, i.e. the bandwidth containing the dominant system modes. The power spectral density plot of the pitch, y_1, and the yaw, y_2, responses (see Fig. 5) to the PRBS input, u_1, signal (Fig. 6) indicates that the dominant resonance modes of the system are located within 0–1 Hz, as expected. The pitch channel $u_1 \rightarrow y_1$ has a main resonant mode at 0.34 Hz, and the yaw channel $u_1 \rightarrow y_2$ at around 0.1 Hz. Hence, a fourth-order model is expected, corresponding to one resonance mode at 0.34 Hz and one rigid-body pitch mode for the $u_1 \rightarrow y_1$ channel. Similarly, a model order of 2 or 4 is anticipated for the $u_1 \rightarrow y_2$ channel owing to the presence of one resonance mode at 0.1 Hz and the yaw rigid-body mode.

Similarly, for the second input, u_2, and second output, y_2, a model order of 2 or 4 is expected corresponding to the normal mode at 0.1 Hz and a rigid-body yaw mode (see Fig. 7). The results of identification of the system modes are summarized in Table 1.

5.2 Parametric modelling

Equipped with the insight gained above, attention is focused on employing parameters in the model to obtain the best system description. A parametric method can be characterized as a mapping from the experimental data to the estimated parameter vector. Such models are often required for control application purposes. With no prior knowledge of sensor or instrument noise, a preliminary

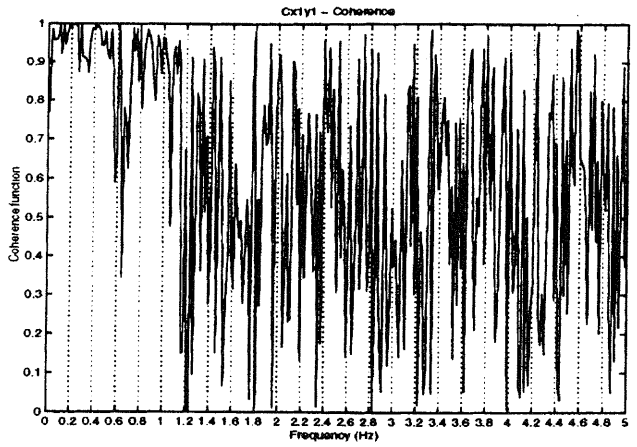

(a) Channel *u1* → *y1*.

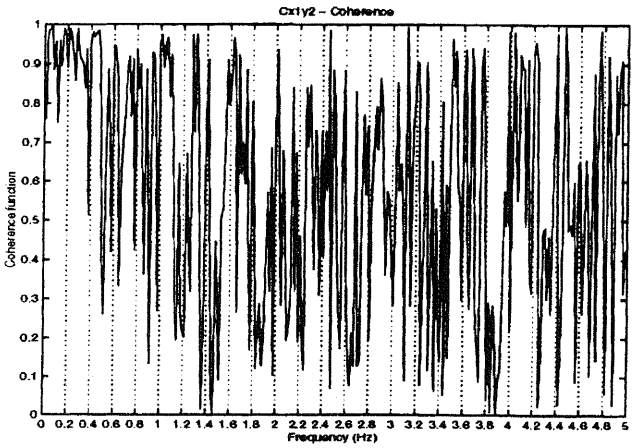

(b) Channel *u1* → *y2*.

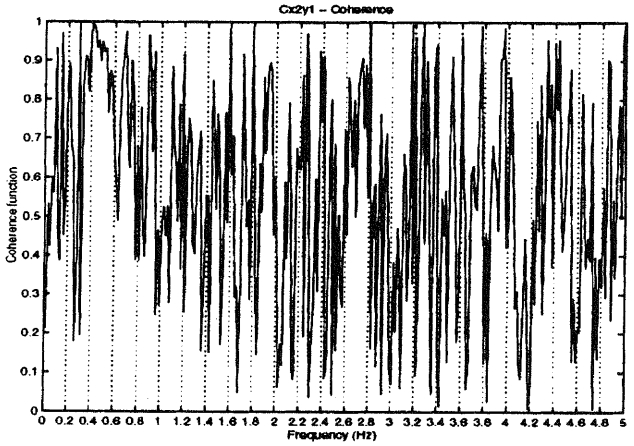

(c) Channel *u2* → *y1*.

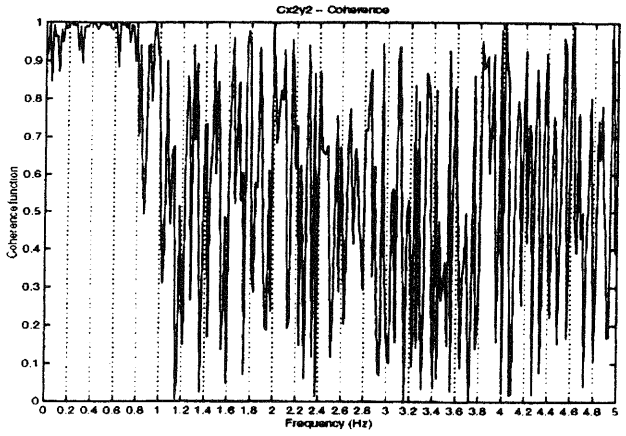

(d) Channel *u2* → *y2*.

Fig. 3 Coherence spectrum: (a) channel $u_1 \rightarrow y_1$; (b) channel $u_1 \rightarrow y_2$; (c) channel $u_2 \rightarrow y_1$; (d) channel $u_2 \rightarrow y_2$

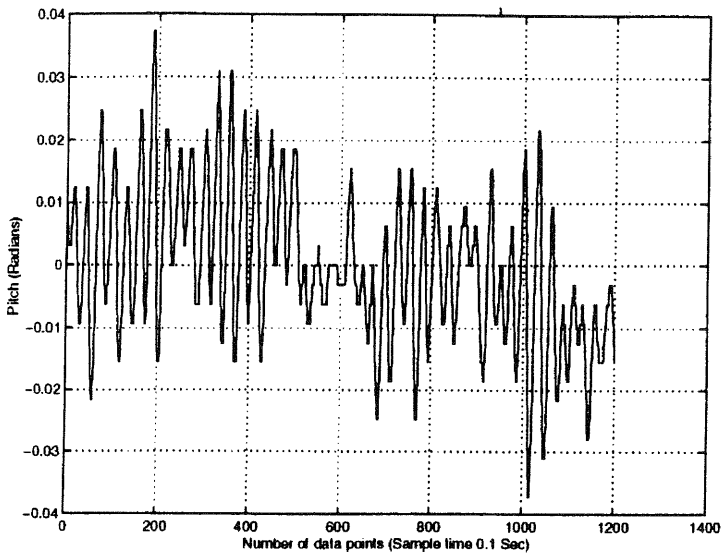

Fig. 4 Pitch response for channel $u_2 \rightarrow y_1$

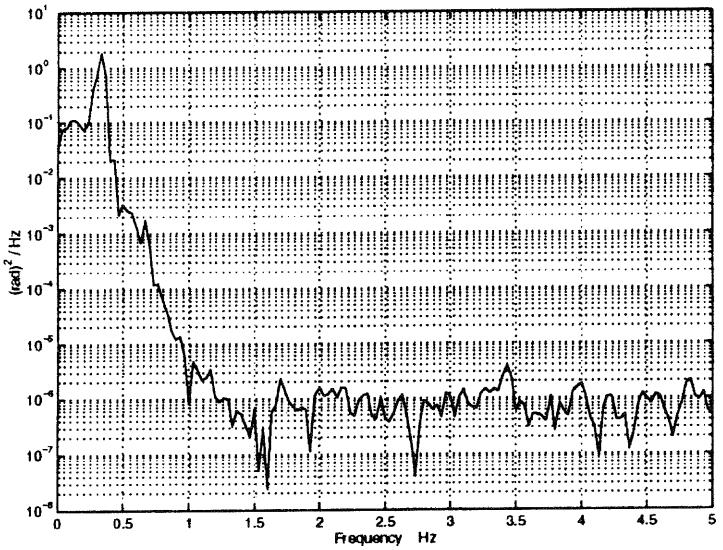

(a) Pitch response, *u1* → *y1*.

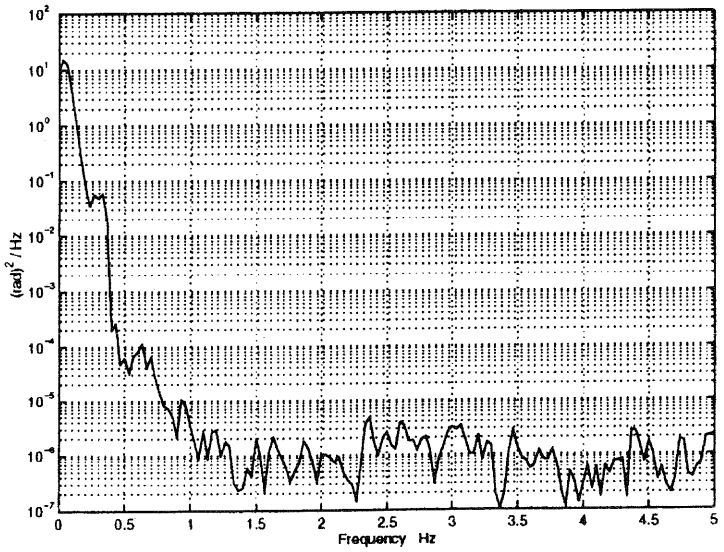

(b) Yaw response, *u1* → *y2*.

Fig. 5 Power spectral density: (a) pitch response, $u_1 \rightarrow y_1$; (b) yaw response, $u_1 \rightarrow y_2$

second-order autoregressive with exogenous input (ARX) model was assumed for the $u_1 \rightarrow y_1$ channel. The autocorrelation of residuals revealed negative correlation at lag 1, indicating the presence of non-white, sensor or external noise. This necessitates estimating the noise statistics. Therefore, the autoregressive moving average with exogenous input (ARMAX) model structure

$$\begin{aligned} y(t) + a_1 y(t-1) + \cdots + a_{n_a} y(t-n_a) \\ = b_1 u(t-1) + \cdots + b_{n_b} u(t-n_b) + e(t) \\ + c_1 e(t-1) + \cdots + c_{n_c} e(t-n_c) \end{aligned} \quad (2)$$

was selected for further analysis, where a_i, b_i and c_i are the parameters to be identified and $e(t)$ is a zero mean white noise. This structure takes into account both the true system and noise models. The ARMAX model was found to be appropriate for all three channels under study.

In the time domain identification, prediction errors or residuals $\varepsilon(t)$ are analysed for arriving at an appropriate model structure. Residuals are the errors observed between the model response and the actual response of the plant to the same excitation. A model structure can be found, iteratively, that minimizes the absolute sum of the residuals.

5.3 Identification

The input signals utilized for identification and cross-validation are depicted in Fig. 8. The corresponding ouput responses for different channels are shown in Figs 9, 11

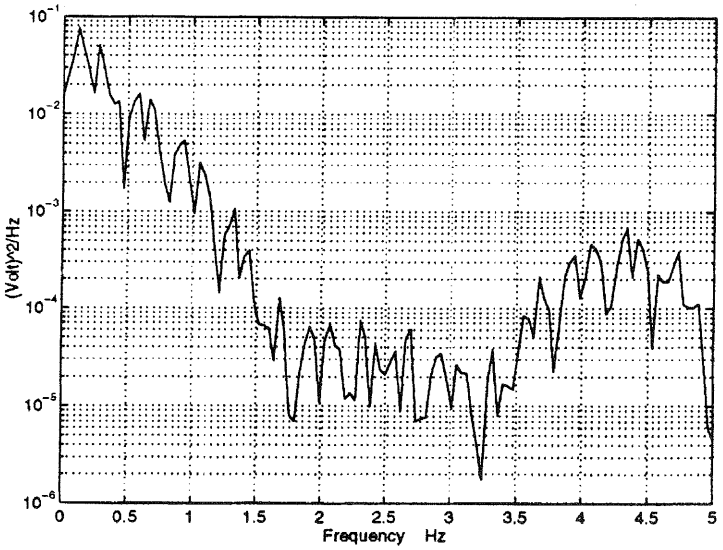

Fig. 6 Spectral density of input u_1

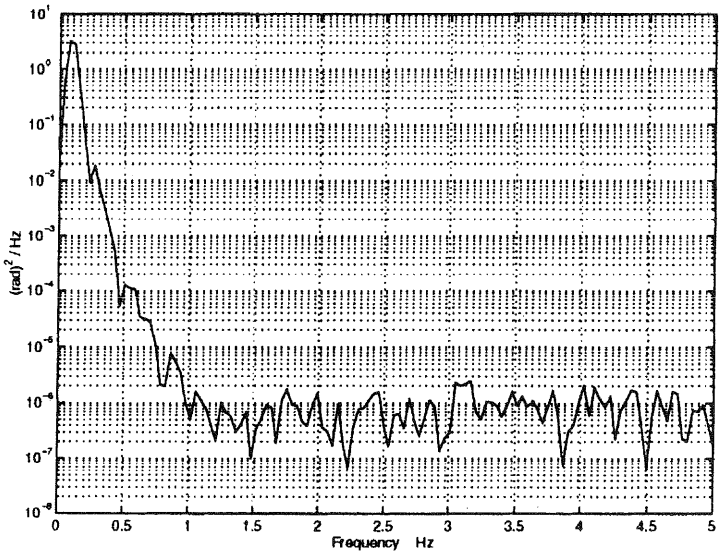

Fig. 7 Power spectral density: yaw response $u_2 \rightarrow y_2$

Table 1 Identified natural frequencies

Channel	Identified system modes
$u_1 \rightarrow y_1$	0.1 and 0.34 Hz
$u_1 \rightarrow y_2$	0.1 Hz
$u_2 \rightarrow y_2$	0.1 Hz
$u_2 \rightarrow y_1$	No cross-coupling

and 12. Referring to Figs 8 and 9, only 600 input–output data points were used for estimation of parameters, while the doublet signal was used for a model cross-validation test for the input u_1 and the output y_1. A fourth-order ARMAX model was found iteratively, using the MATLAB system identification toolbox [**22**].

Figure 10a depicts the autocorrelation test of the residuals, signifying that the noise has been modelled adequately as well as that the model order is appropriate. The cross-correlation function between the residuals and the input is shown in Fig. 10b, which is well within the 95 per cent confidence band marked by the dotted lines. Independence between the residuals and past input is imperative, and this is a measure of proper estimation of time delays.

An analogous procedure was repeated for channels $u_1 \rightarrow y_2$ and $u_2 \rightarrow y_2$. The test data used for identification

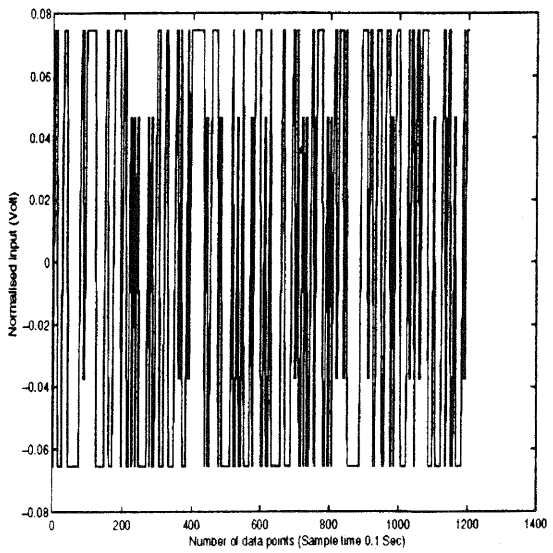

a) PRBS input for system identification

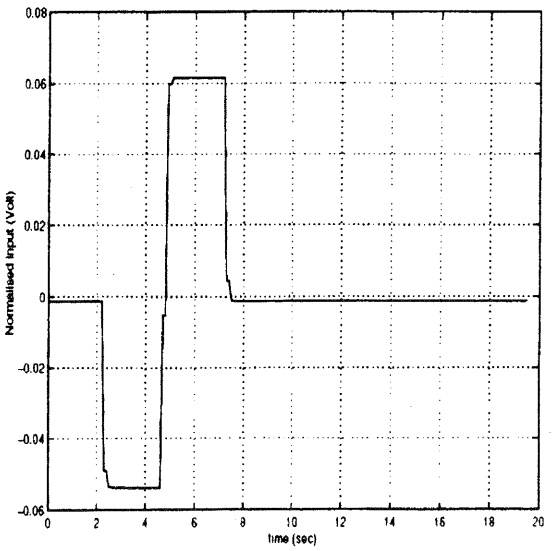

b) Doublet input for cross- validation

Fig. 8 Input signals used for modelling

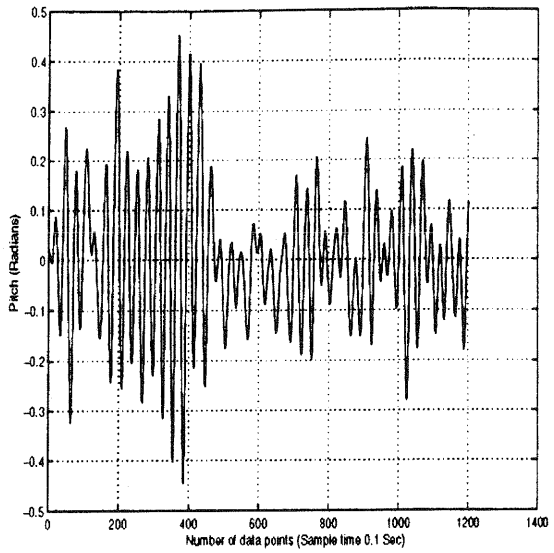

(a) System response to PRBS input.

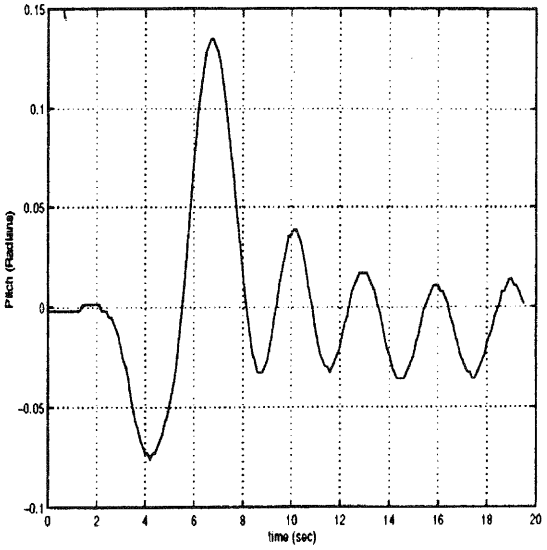

(b) System response to doublet.

Fig. 9 Output test data for channel $u_1 \rightarrow y_1$

are shown in Figs 8, 11 and 12. Finally, the residual test for the identified models is illustrated in Figs 13 and 14.

5.4 Time domain validation

Verification is a key final step in a system identification process, which assesses the predictive quality of the extracted model. Data not used in the estimation are selected in order to ensure that the model is not tuned to specific data records or input forms. In this cross-validation study, the model is tested against a doublet and shown in Fig. 8b. In Fig. 15, the simulated model output and the experimental output are compared for the $u_1 \rightarrow y_1$ channel. The predictive capability of the model is quite good, as the model closely traces the plant output.

However, as evident from Fig. 16, the model response for $u_1 \rightarrow y_2$ is not so good. This is most likely due to the unrestricted movement in the yaw plane, leading to non-linearity. Further analysis is given in Section 5.5. Excellent model response was obtained for the $u_2 \rightarrow y_2$ channel, as illustrated in Fig. 17.

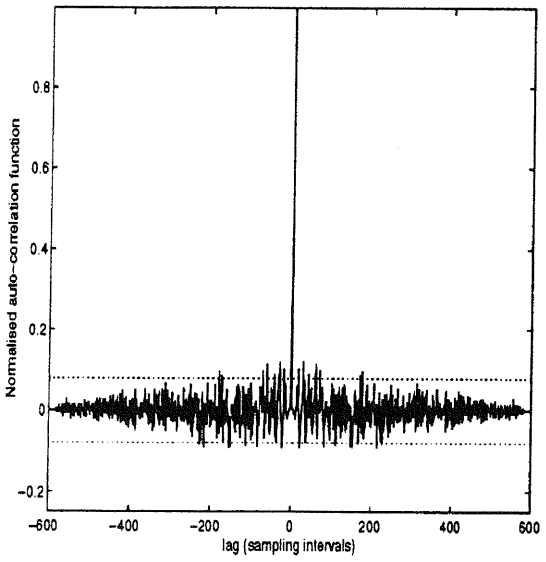

(a) Auto-correlation of residuals

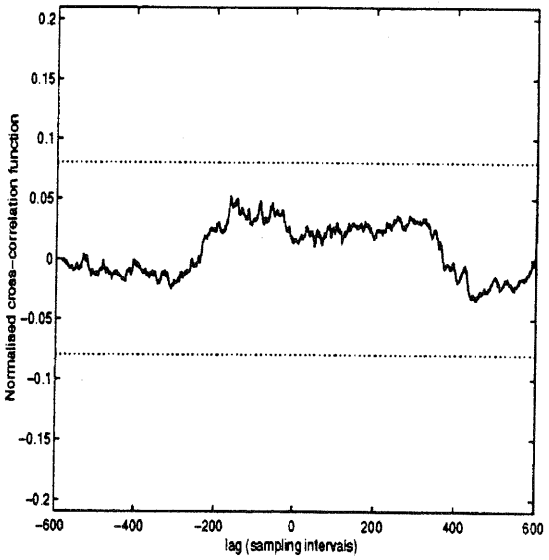

(b) Cross-correlation of residuals

Fig. 10 Residual test for channel $u_1 \rightarrow y_1$

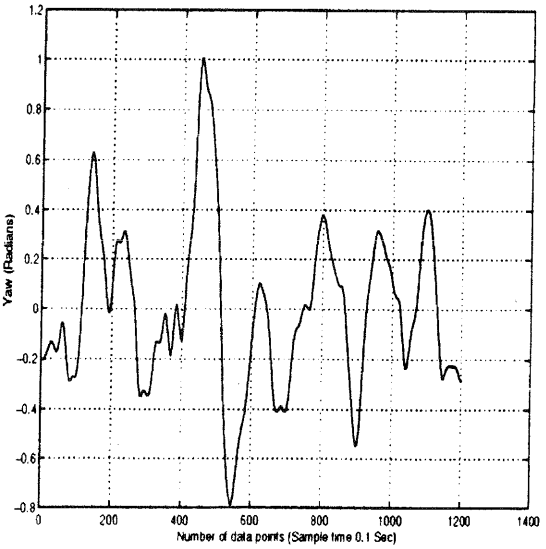

(a) System response to PRBS input.

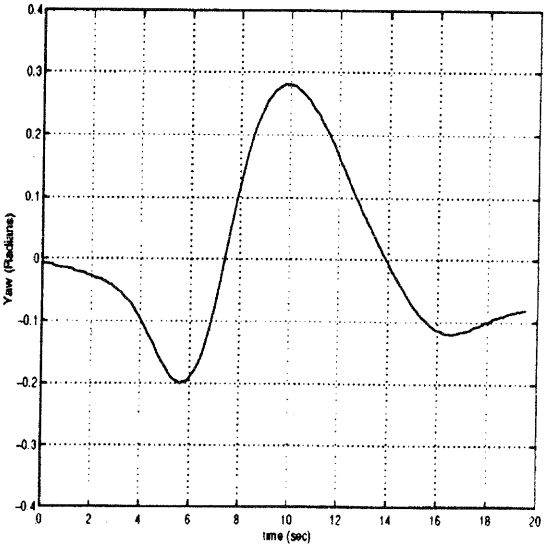

(b) System response to doublet.

Fig. 11 Output test data for channel $u_1 \rightarrow y_2$

5.5 Frequency domain validation

In frequency domain cross-validation tests, emphasis is placed on the ability of the model to predict system modes. Power spectral density plots of the plant and model outputs are superimposed in Fig. 18 for the $u_1 \rightarrow y_1$ and $u_1 \rightarrow y_2$ channels and in Fig. 19 for the $u_2 \rightarrow y_2$ channel. Note the presence of one common mode at 0.1 Hz in the $u_1 \rightarrow y_2$ and $u_2 \rightarrow y_2$ channels. This is because both channels describe the yaw motion although excited by different inputs. It is noted that the dominant modes of the model and the plant coincide quite well for the $u_1 \rightarrow y_1$ channel, implying good model predicting capability of the important system dynamics. However, the spectral plot of the model indicates a slightly higher magnitude for the $u_1 \rightarrow y_2$ channel (see Fig. 18b). This discrepancy could well be due to the non-linearity introduced because of unconstrained yaw movement. Also, the coherence spectrum shown in Fig. 3b indicates a coherence lower than 1 in the proximity of the dominant mode, i.e. 0.1 Hz. This could well be due to one or a combination of reasons mentioned in Section 4.3. Extraneous noise cannot be suspected, as coherence functions of other channels are fairly close to unity. At sharply peaked system resonance modes, the coherence

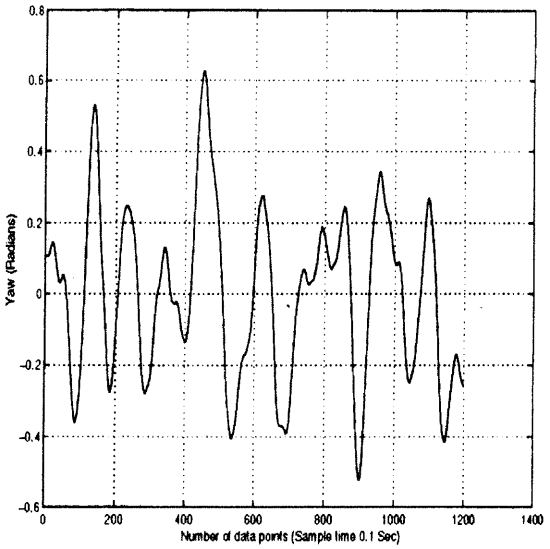

(a) System response to PRBS input.

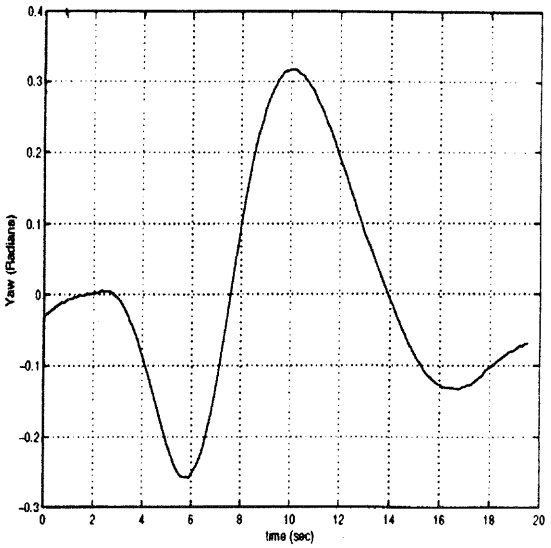

(b) System response to doublet.

Fig. 12 Output test data: (a) channel $u_1 \rightarrow y_2$; (b) channel $u_2 \rightarrow y_2$

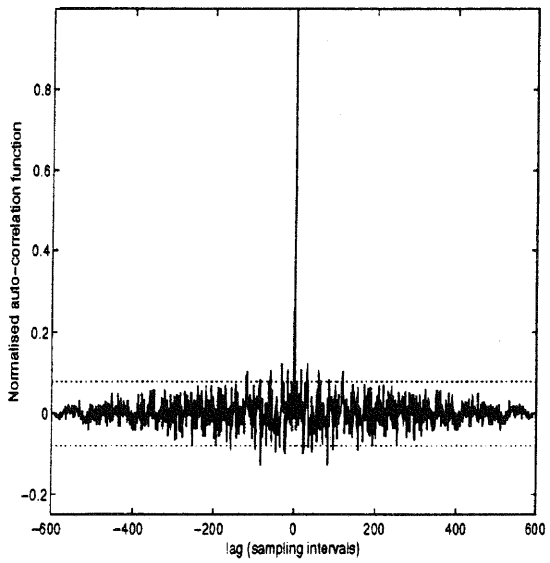

(a) Auto-correlation of residuals

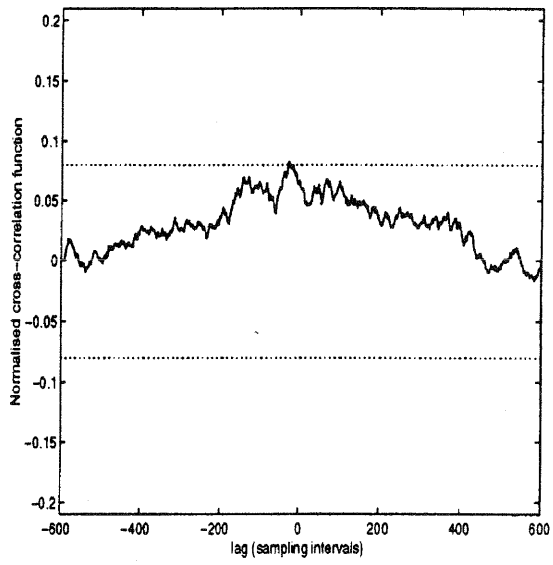

(b) Cross-correlation of residuals

Fig. 13 Residual test for channel $u_1 \rightarrow y_2$

functions $-\gamma^2_{xy}(f)$ will usually peak sharply corresponding to these resonance frequencies, because the signal–noise ratio is highest at these frequencies. If $\gamma^2_{xy}(f)$ at such frequencies does not peak sharply, or worse still notches, then system non-linearities and resolution bias errors might be suspected [**21**]. Bias error is an unlikely candidate, as enough data points were used for coherence estimation/calculation. Thus, from the analysis, this test indicates that there might be a slight non-linear relationship between u_1 and y_2, which may be the cause of poor model fit. However, the effect of external disturbances is not ruled out either.

The spectral plot in Fig. 19 for the $u_2 \rightarrow y_2$ channel also illustrates excellent agreement between the plant and the model modes in the frequency range of interest, i.e. 0–1 Hz. Thus, from the foregoing analysis it can be concluded that the models have captured the important plant dynamics quite well.

6 INTERPRETING THE BLACK BOX MODEL

In this work, the black box approach is adopted in order to circumvent the tedious mathematical modelling process.

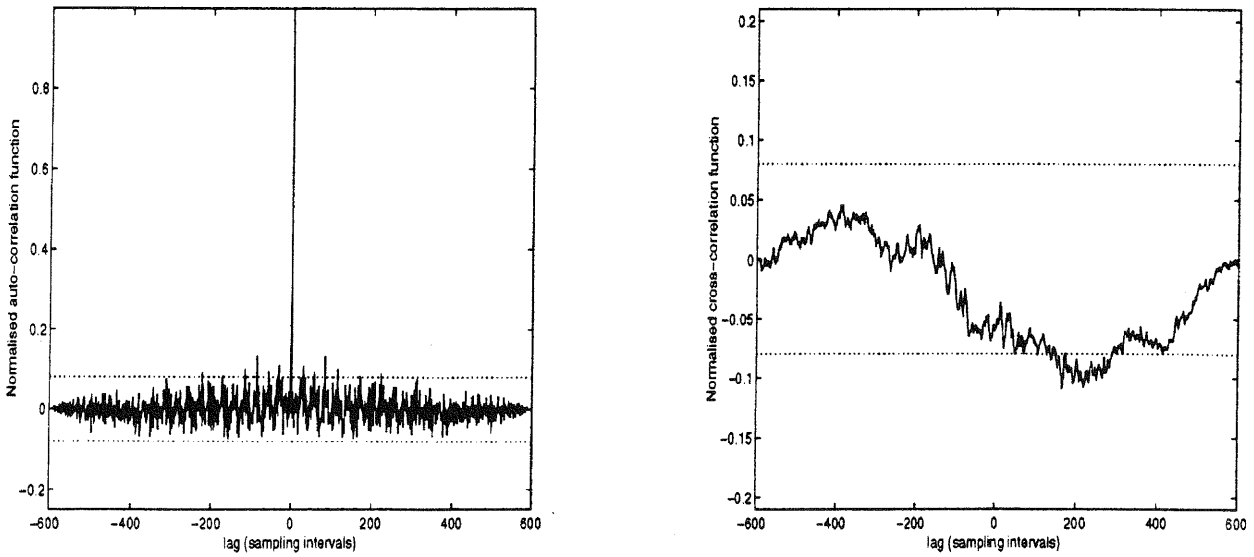

(a) Auto-correlation of residuals (b) Cross-correlation of residuals

Fig. 14 Residual test for channel $u_2 \rightarrow y_2$

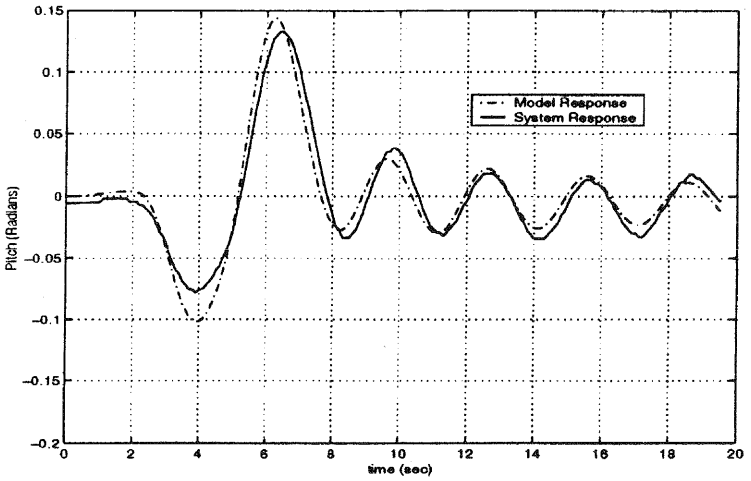

Fig. 15 Response to a doublet, $u_1 \rightarrow y_1$

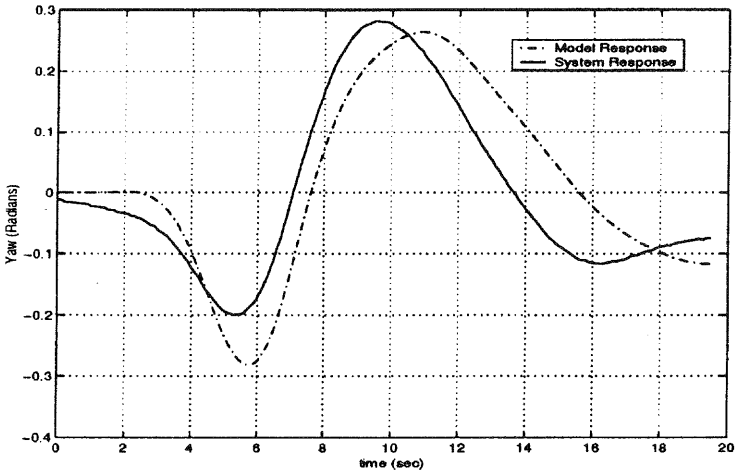

Fig. 16 Response to a doublet, $u_1 \rightarrow y_2$

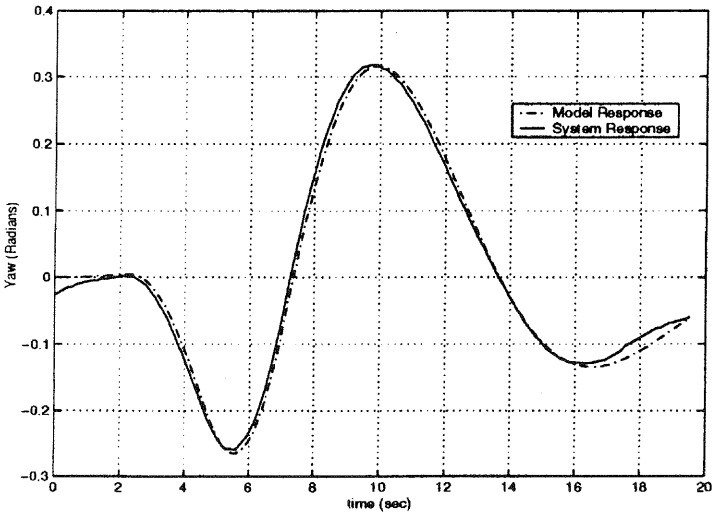

Fig. 17 Response to a doublet, $u_2 \rightarrow y_2$

However, it may be desirable to give physical meaning to the model coefficients and understand their influence on the vehicle motion. Such an understanding would aid in the system analysis, controller design and even redesign or modification of the vehicle component(s) to achieve the desired system dynamic characteristics. Therefore, in this section an attempt is made to interpret the extracted black box model, that is, to relate the parameters of the model to the actual system dynamic behaviour.

If only an input–output representation, for instance of the $u_1 \rightarrow y_1$ channel (pitch axis) of the TRMS, is of interest, then a discrete-time transfer function can be obtained from the identified parametric model as

$$\frac{y_1}{u_1} = \frac{-0.0007z^3 + 0.007z^2 + 0.0001z + 0.006}{z^4 - 2.372z^3 + 1.465z^2 + 0.2673z - 0.351} \tag{3}$$

where y_1 represents the pitch angle (in radians) and u_1 is the main rotor input (in volts).

The parameters of the transfer function in equation (3) have no physical meaning, but the dynamic characteristics of the system depend directly upon them, and it would be interesting to make it evident in the structure. Factoring the denominator polynomial of equation (3) yields

$$\frac{y_1}{u_1} = \frac{(z-10.09)(z+0.0491+0.92i)(z+0.0491-0.92i)}{(z-0.8488)(z-0.42)(z-0.971+0.21i)(z-0.971-0.21i)} \tag{4}$$

implying that the system has complex poles. Thus, bringing into evidence the (almost) unstable oscillatory mode, which is a significant dynamic characteristic of the TRMS and also of a helicopter in hover. The oscillatory or vibrational motion is imparted to the system due to flexible structural component(s). The complex poles in the characteristic equation are therefore directly related to the physical properties of the structural material. The transfer functions for the $u_1 \rightarrow y_2$ and $u_2 \rightarrow y_2$ channels are

$$\frac{y_2}{u_1} = \frac{(z-0.6971)(z-0.0515+1.8236i)(z-0.0515-1.8236i)}{(z-0.9573)(z+0.5961)(z-0.9773+0.0492i) \times (z-0.9773-0.0492i)} \tag{5}$$

$$\frac{y_2}{u_2} = \frac{(z+1.48)(z-0.91+1.5089i)(z-0.91-1.5089i)}{(z-0.773)(z+0.582)(z-0.982+0.0497i) \times (z-0.982-0.0497i)} \tag{6}$$

where y_2 represents the pitch angle (in radians) and u_2 is the tail rotor input (in volts). Similarly, complex poles in equations (5) and (6) arise owing to the excitation of the elastic TRMS modes in the yaw plane by the inputs u_1 and u_2 respectively.

For a 1 DOF purely rigid body, it takes two state variables (one position and one velocity) to describe the motion of the body. Thus, the real poles in equation (4) represent two state variables that describe the rigid-body motion, namely the pitch angle (position) and pitch velocity. In an analogous manner, rigid-body motions in the yaw plane, i.e. yaw angle and yaw velocity due to coupled $u_1 \rightarrow y_2$ motion and the $u_2 \rightarrow y_2$ channel, are represented by the real poles of equations (5) and (6) respectively. Note that the system is non-minimum phase, with zeros outside the unit circle. Interpretation of the black box model thus brings to the fore similar information to that obtained from the mathematical modelling process.

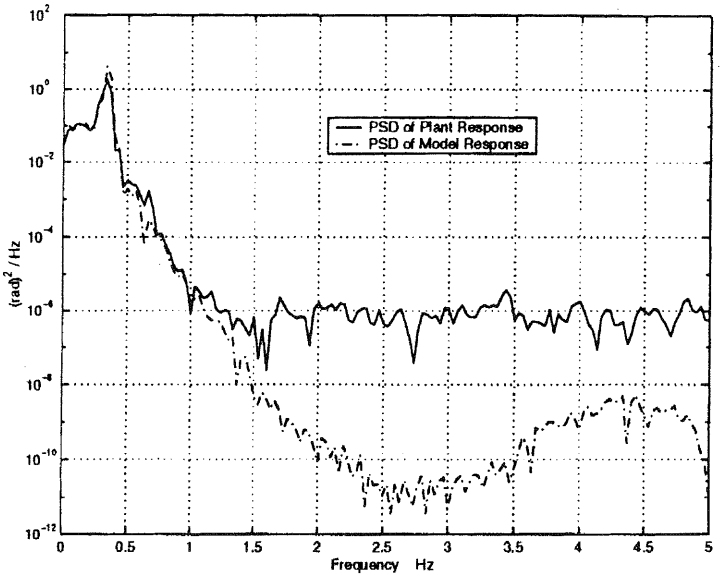

(a) Pitch response, *u1* → *y1*.

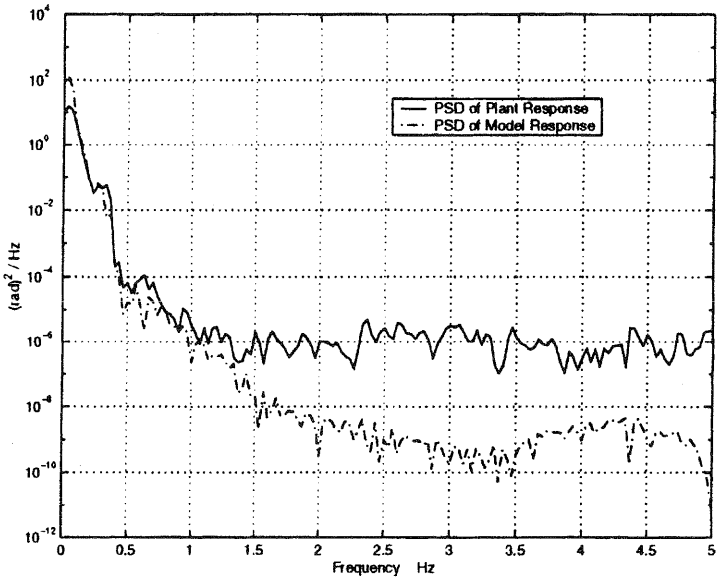

(b) Yaw response, *u1* → *y2*.

Fig. 18 Power spectral density: (a) pitch response, $u_1 \rightarrow y_1$; (b) yaw response, $u_1 \rightarrow y_2$

7 CONCLUSION

System identification is an ideal tool for modelling non-standard aircraft configurations whose flight mechanics is not well understood. Linear system identification techniques have been investigated for modelling a 2 DOF MIMO TRMS in hover, the dynamics of which resemble that of a helicopter. Time domain linear system identification has been employed to obtain the parametric system models. These transfer functions are to be used for control applications. Both time and frequency domain analyses have been utilized to investigate and develop confidence in the obtained models. The frequency domain verification method is a useful tool in the validation of extracted parametric models. It allows high-fidelity verification of dynamic characteristics over a frequency range of interest. The extracted models have predicted the system behaviour well. The TRMS has a strong coupling between the $u_1 \rightarrow y_1$, $u_1 \rightarrow y_2$ and $u_2 \rightarrow y_2$ channels. However, there is a weak interaction in the $u_2 \rightarrow y_1$ channel, and hence this path was omitted and no attempt was made to fit the model for this route. Moreover, identification of $u_1 \rightarrow y_2$ was imperfect which may be due to non-linearity and external disturbance. However, it is presumed that the resulting model is suitable for controller design, and accordingly the modelling approach presented is suitable for complex new-generation air vehicles.

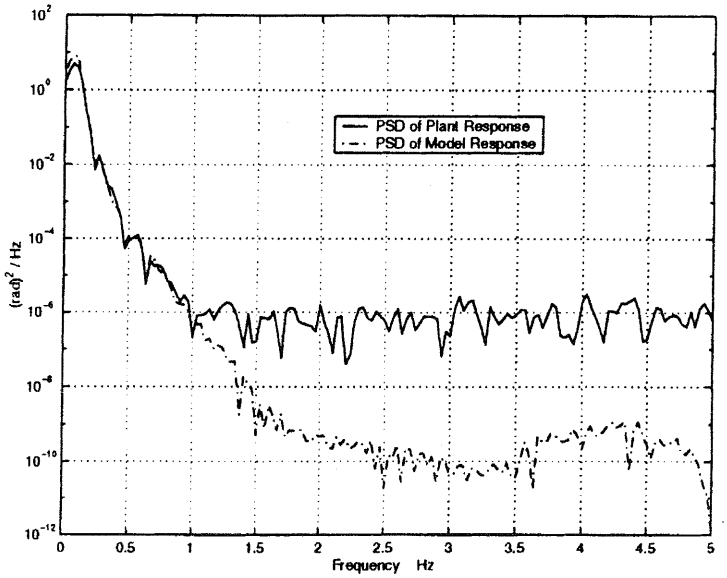

Fig. 19 Power spectral density: yaw response $u_2 \rightarrow y_2$

ACKNOWLEDGEMENTS

S. M. Ahmad gratefully acknowledges the financial support of the University of Sheffield. The authors would like to thank Dr H.A.Thompson, Manager, Rolls-Royce (UTC, the University of Sheffield), for many valuable comments on helicopter dynamics. Thanks are also due to Prof. S. Billings and Dr Zi-Qiang Lang for useful discussions on MIMO system identification.

REFERENCES

1 *Methods for Aircraft State and Parameter Identification*, 1974 (AGARD, NASA Research Centre, Hampton, Virginia).

2 **Bruce, P. D., Silva, J. E. F.** and **Kellet, M. G.** Maximum likelihood identification of linear aircraft dynamics using a hybrid genetic algorithm. In Proceedings of AIAA 36th Aerospace Sciences Conference, Reno, Nevada, 1998.

3 **Kaminer, I., Pascoal, A., Hallberg, E.** and **Silvestre, C.** Trajectory tracking for autonomous vehicles: an integrated approach to guidance and control. *Am. Inst. Aeronaut. Astronaut. J. Guidance, Control, and Dynamics*, 1998, **21**, 29–38.

4 **Hallberg, E., Kaminer, I.** and **Pascoal, A.** Development of a flight test system for unmanned air vehicles. *IEEE Control Syst.*, 1999, **19**(1), 55–65.

5 **Atkins, E. M., Miller, R. H., Pelt, T. V., Shaw, K. D., Ribbens, W. B., Washabaugh, P. D.** and **Bernstein, D. S.** SOLUS: an autonomous aircraft for flight control and trajectory planning research. In Proceedings of American Control Conference, Philadelphia, Pennsylvania, 1998, Vol. 2, pp. 689–693.

6 **Linehan, R. D., Burnham, K. J.** and **James, D. J. G.** 4-Dimensional control of a remotely piloted vehicle. In Proceedings of UKACC, 1996, pp. 770–775.

7 *Company R&D History*, 1997 (Freewing Aerial Robotics Corp., College Station, Texas); www.freewing.com.

8 **Van Nieuwstadt, M. J.** and **Murray, R. M.** Rapid hover-to-forward-flight transitions for a thrust-vectored aircraft. *Am. Inst. Aeronaut. Astronaut. J. Guidance, Control, and Dynamics*, 1998, **21**, 93–100.

9 **Morris, J. C., Van Nieuwstadt, M. J.** and **Pascale, B.** Identification and control of a model helicopter in hover. In Proceedings of American Control Conference, Baltimore, Maryland, 1994, Vol. 2, pp. 1238–1242.

10 **Houston, S. S.** Identification of autogyro longitudinal stability and control characteristics. *Am. Inst. Aeronaut. Astronaut. J. Guidance, Control, and Dynamics*, 1998, **21**, 391–399.

11 **Werner, H.** and **Meister, T.** Robust control of a laboratory aircraft model via fast output sampling. *Control Engng Practice*, 1999, **7**, 305–313.

12 **Blythe, P. W.** and **Chamitoff, G.** Estimation of aircrafts aerodynamic coefficients using recurrent neural networks. In Proceedings of 2nd Pacific International Conference on *Aerospace Science and Technology*, 1995.

13 **Haley, P.** and **Soloway, D.** Generalized predictive control for active flutter suppression. *IEEE Control Syst.*, 1997, 64–70.

14 **Ahmad, S. M., Chipperfield, A. J.** and **Tokhi, M. O.** Modelling and control of a twin rotor multi-input multi-output system. In Proceedings of the American Control Conference, Chicago, Illinois, 28–30 June 2000, pp. 1720–1724.

15 **Ahmad, S. M., Chipperfield, A. J.** and **Tokhi, M. O.** Dynamic modelling of a two degree-of-freedom twin rotor multi-input multi-output system. In UKACC International Conference on *Control-2000,* Cambridge, 4–7 September 2000.

16 *Twin Rotor MIMO System. Manual 33-007-0*, 1996 (Feedback Instruments Limited, Sussex).

17 **Patton, R., Miles, M.** and **Taylor, P.** Design and application of test signals for helicopter model validation in the frequency domain. In *Perturbation Signals for System Identification* (Ed. K. Godfrey), 1993, pp. 298–320 (Prentice-Hall, UK).

18 **Ljung, L.** *System Identification: Theory for the User*, 1987, p. 386 (Prentice-Hall).

19 **Wellstead, P. E.** and **Zarrop, M. B.** *Self-Tuning Systems: Control and Signal Processing*, 1991, pp. 126–128 (John Wiley, Chichester).

20 **Ahmad, S. M., Chipperfield, A. J.** and **Tokhi, M. O.** System identification of a one degree-of-freedom twin rotor multi-input multi-output system. In Proceedings of International Conference on *Computer and Information Technology*, Sylhet, Bangladesh, 1999, pp. 94–98 (SUST).

21 **Bendat, J. S.** and **Piersol, A. G.** *Engineering Application of Correlation and Spectral Analysis*, 1980, pp. 83–84 (John Wiley).

22 **Ljung, L.** *System Identification Toolbox*, 1991 (The MathWorks Inc., Natick, Massachusetts).